1-14-2019

Late Pleistocene Glaciation in the Mosquito Range, Colorado, U.S.A.: Chronology and Climate

Keith A. Brugger
University of Minnesota, Morris, bruggeka@morris.umn.edu

Benjamin J.C. Laabs
North Dakota State University--Fargo

Alexander Reimers
North Dakota State University--Fargo

Noah Bensen
University of Minnesota, Morris, bense034@morris.umn.edu

FINAL VERSION *ACCEPTED* FOR PUBLICATION IN THE JOURNAL OF QUATERNARY SCIENCE 1/14/19 *(Supporting information omitted)*

Late Pleistocene Glaciation in the Mosquito Range, Colorado, U.S.A.: Chronology and Climate

Keith A. Brugger[1], Benjamin Laabs[2], Alexander Reimers[2], Noah Bensen[3]

[1]Geology Discipline, University of Minnesota, Morris, Morris, MN, U.S.A. 56267
[2]Department of Geosciences, North Dakota State University, Fargo, ND, U.S.A 58102
[3]Chemistry Discipline, University of Minnesota, Morris, Morris, MN, U.S.A. 56267

Abstract

New cosmogenic ^{10}Be surface exposure ages from seventeen moraine boulders in the Mosquito Range suggest that glaciers were at their late Pleistocene (Pinedale) maximum extent at ~21–20 ka, and that ice recession commenced prior to ~17 ka. These age limits suggest that the Pinedale Glaciation was synchronous within the Colorado Rocky Mountain region. Locally, the previous (Bull Lake) glaciation appears to have occurred no later than 117 ka, possibly ~130 ka allowing for reasonable rock weathering rates. Temperature-index modeling is used to determine the magnitude of temperature depression required to maintain steady-state mass balances of seven reconstructed glaciers at their maximum extent. Assuming no significant differences in precipitation compared to modern values, mean annual temperatures were ~8.1 and 7.5 °C cooler, respectively, on the eastern and western slopes of the range with quantifiable uncertainties of +0.8/–0.9 °C. If an average temperature depression of 7.8 °C is assumed for the entire range, precipitation differences - that today are 15-30% greater on the eastern slope due to the influence of winter/early spring snowfall - might have been enhanced. The temperature depressions inferred here are consistent with similarly derived values elsewhere in the Colorado Rockies and those inferred from regional-scale climate modeling.

Keywords: Colorado; Pinedale glaciation; cosmogenic exposure dating; glacial chronology; paleoclimate

Introduction

The precise timing of Late Pleistocene glacial advances and deglaciation in the western United States and the magnitude of their respective causative forcings inform our understanding of paleoclimate dynamics (Licciardi *et al*., 2004; Thackray, 2008). Despite the increasing number of well-constrained glacial chronologies across the montane western U.S. (e.g. Phillips *et al*., 1990, 1996, 2009; Gosse *et al*., 1995; Licciardi *et al*., 2001, 2004; Leonard *et al*., 2017a; Licciardi and Pierce, 2018), additional studies are needed in order to better define spatial and temporal patterns of glacier behavior and climate during the last Pleistocene glaciation. Specifically, asynchronous glacier behavior might reveal the influence of secondary climatic factors or internal dynamics affecting response that are superimposed on global-scale drivers of climate change (e.g insolation and atmospheric CO_2). These include differences in glacier hypsometry, local or microclimate (i.e. sub-regional energy and mass balances), and/or glacier response times (e.g. Thackray, 2008; Laabs *et al*., 2009; Young *et al*., 2011). Glacial chronologies also provide a temporal context for proxies of Late Pleistocene climate inferred from glacier fluctuations. Because the Last Glacial Maximum (LGM), in particular, represents a unique climatic state very different than those of the subsequent 20 ka, glacial records provide important information unavailable from many other sedimentary and biological records (e.g. pollen spectra) because of limits of the length of the respective records or geographic coverage. Thus glacial chronologies and their value for understanding LGM climate represent fundamental data that are critical in evaluating the skill of models (so-called “hindcasting”) used to project future global change (Braconnot *et al*., 2012; Flato *et al*., 2013; Kageyama *et al*., 2017). The increasing number of precise glacial chronologies notwithstanding, few (e.g. Ward *et al*., 2009; Leonard *et al*., 2017a) have been integrated with modeling approaches to infer details concerning climate change during the last glaciation.

Addressing the need for both additional glacial chronologies and climate reconstructions in the Rocky Mountains, we present here new cosmogenic ^{10}Be surface-exposure ages of moraines and model-derived limits on Late Pleistocene climate from the Mosquito Range, Colorado, an area that has received little attention with respect to its glacial history. Exposure ages obtained from moraine boulders indicate glaciers achieved their last Pleistocene maximum extent ca. 21–20 ka and overall deglaciation commenced by 17 ka. Our results suggest the timing of moraine occupation in the Mosquito Range agrees with recent Pleistocene glacial chronologies developed in adjacent ranges in Colorado. Limits on the last glacial climate in the study area are inferred from temperature-index modeling, which determines temperature depressions required to maintain steady-state mass-balances of reconstructed paleoglaciers. Our estimates of temperature depression in the Mosquito Range are in excellent agreement with those similarly determined in the region.

Study Area

The Mosquito Range is a north-south trending range bordered by the upper Arkansas River valley and Sawatch Range to the west and South Park and the southern Front Range to the east (Fig. 1). The Arkansas River valley is a topographic expression of the northernmost extent of the Rio Grande Rift that became tectonically active ca. 30–25 Ma (Kellogg *et al*., 2017). Many peaks exceed 4000 m and features typical of alpine glaciation and periglacial activity characterize landscapes at higher elevations. Structurally the range is cored by Precambrian crystalline rocks unconformably overlain by complexly faulted and folded Paleozoic clastics and carbonates that were later intruded by a suite of Tertiary sills, dikes, and small plutons (McCalpin *et al*., 2012a, b; Kellogg *et al*., 2017).

Late-Quaternary glaciation in the Mosquito Range was characterized by extensive valley glacier systems (Fig. 2a). These systems were to a large degree interconnected either by virtue of common ice fields and/or pervasive ice divides. The ice fields also solely supported several small ice lobes. In some locations glaciers in adjacent valleys coalesced to form composite termini. Glaciers were more extensive in the northern part of the range where ice masses were contiguous with ice sourced from the Tenmile Range and other isolated peaks. An east-west asymmetry with respect to glacier length and area existed during the LGM that becomes more pronounced in the central and southern part of the range. Glaciers had both greater lengths and surface areas on the eastern slope. Although the elevations of catchment areas are comparable (~3600–3800 m), glaciers there terminated at lower elevations than did those on the western slopes. Well-preserved terminal and lateral moraines of the last (Pinedale) and penultimate (Bull Lake) glaciations are common at the mouths of glaciated valleys, and in most are delineated on bedrock maps (Widmann *et al*., 2007; McCalpin *et al*., 2012a, b; Bohannon and Ruleman, 2013; Kellogg *et al*., 2017). The relative ages of these moraines can generally be distinguished by morphostratigraphic criteria (e.g. boulder abundance and freshness, sharpness of moraine crests, etc.). In these valleys recessional moraines of the Pinedale Glaciation are also evident.

Modern climate in the Mosquito Range is continental, with mean annual temperatures (MAT) of ~2 °C at the mountain fronts (~3000 m) and ~-5 °C at the highest elevations (>4000 m). (Data from the stations shown in Fig. 1 are derived available through the Western Regional Climate Center, http://wrcc.dri.edu, and the National Water and Climate Center, http://wcc.nrcs.usda.gov, in addition to that provided by the PRISM Climate Group, Oregon State University, http://prism.oregonstate.edu.) Mean January and July temperatures typically deviate from the mean annual temperature by ±10 °C irrespective of elevation. For a given elevation, MATs tend to be on average ~1 °C warmer on the eastern slope of the range at elevations between 3000 and 3700 m. At the highest elevations (>3700), MAT are slightly cooler by ~ 0.5 °C.

Mean annual precipitation (MAP) varies from ~40 cm at the lowest elevation of the range to ~120 cm on the high peaks, averaging ~76 cm. The monthly/seasonal distribution of precipitation varies over the range; however, the general pattern is bimodal with an early maximum in late winter/early spring and a later maximum corresponding to mid-to-late summer (Fig. 3a). The earlier maximum is more muted at the lowest elevations but at higher elevations it is comparable to or greater than the later maximum.

For much of the year, moist Pacific air is delivered to the Colorado Rocky Mountains by prevailing westerly flow. The Mosquito Range, being essentially on the eastern boundary, therefore receives less precipitation than ranges farther west. However, during the late winter and early spring, synoptic circulation patterns cause upslope precipitation of southeasterly Gulf of Mexico-derived moisture. This disproportionally affects the eastern slopes. Mid- to late summer precipitation is associated with the North American monsoon (Higgins *et al*., 1997) that brings moisture from the Gulfs of both Mexico and California. The PRISM model yields an area-averaged value for MAP for the eastern slope of ~0.8 m while that for the western slope is ~0.7 m. Given similar elevations, available station records also suggest the eastern slope receives ~0.1 m more precipitation annually than does the western slope. More significantly for this study, winter precipitation (October-April) at elevations between 3000 and 3500 m (Fig. 3b) is ~13% greater on the eastern slope. Disregarding the Fremont Pass SNOTEL site that appears to be anomalous, this disparity increases to ~20%. Extrapolation of the respective trends suggests that at higher elevations (3500–4200 m) the eastern slope could receive as much as 30% more precipitation during the winter.

Methods

Cosmogenic ^{10}Be exposure dating

Ten boulders from mapped terminal moraine complexes of the Pinedale glaciation in three glaciated valleys were sampled for exposure ages, specifically in the valleys of Iowa Gulch, Twelvemile Creek, and Fourmile Creek (Fig 4). In Big Union Creek, four boulders were sampled from a moraine that was/is interpreted as being deposited during a recessional stillstand or minor readvance of ice after the terminal moraine was abandoned. Sampling of the terminal moraine in this valley, about one kilometer downvalley, was avoided because of its poor preservation and lack of suitable boulders. Similarly, the *only* boulder suitable and/or accessible for sampling in the Sacramento valley was on the distal slope of a recessional moraine (Fig. 4). Additionally, two boulders on a moraine segment mapped as pre-Pinedale in the Iowa Gulch valley (Kellogg *et al*., 2017) were sampled. Boulders selected for sampling were located on or as close to moraine crests as possible, and all were granitic lithologies. Where possible, samples were collected from the tops of boulders standing >1 m over the moraine surface, however boulders having heights as little as ~0.4 m were also sampled. Preference was given to boulders exhibiting smooth, polished surfaces but given the coarse nature of the lithologies some sampled boulders did not meet this criterion. Large boulders suitable for sampling on several other moraine segments preserved in the study area were extremely scarce. The reason for this scarcity is unclear, but agreement among exposure ages for each sampled moraine crest suggests that boulder removal or degradation by weathering and erosion has been minimal. Moreover, some moraines in the study area were on private property and were therefore not accessible for sampling. Altogether, seventeen samples were ultimately prepared for cosmogenic isotope analyses and submitted for ^{10}Be/^{9}Be measurement by accelerator mass spectrometry; see Supporting Information for details concerning sample information, processing, and calculation of ^{10}Be exposure ages.

Glacier reconstruction

Field mapping of glacial features to verify and augment those shown on existing geologic maps, examination of topographic maps and digital elevation models, and use of Google Earth® imagery allowed for the determination of the maximum extents of seven paleoglaciers (Fig. 2) on the basis of lateral-terminal moraine complexes and the upper limits of glacial erosion. Ice surface contours were reconstructed by considering mapped ice limits, flow patterns delineated by large-scale erosional forms (e.g. valley trends, streamlined bedrock, roche moutonnées), and general convergent and divergent flow in the accumulation and ablations area respectively. Contours were adjusted iteratively so that reconstructed ice surface slopes were sub-parallel to those of the valley and to ensure driving stresses τ were between 50 and 150 kPa commonly measured on modern glaciers (Cuffey and Paterson 2010). Stresses were calculated using:

$$\tau = S_f \rho g h \sin\alpha \tag{1}$$

where ρ is the density of ice, g is gravitational acceleration, h is ice thickness, α is the slope of the ice surface, and S_f is a shape factor to account for drag of the valley sides (Nye, 1965). The surface slope was averaged over distances of $10h$ to account for longitudinal stress gradients (Bindschadler *et al.*, 1977; Cuffey and Paterson, 2010).

Temperature-index modeling

The temperature-index model (TM) used here is a modified version of what was presented in Brugger (2010). In short, the TM is used to find the temperature and precipitation changes required to maintain steady-state mass-balances of the reconstructed glaciers. To this end an approach was sought that minimized tuning of model parameters.

The variation of the *annual* specific mass-balance (i.e., at a point) b_n with elevation z is simulated by:

$$b_n(z) = \int_{t_1}^{t_2} \left(P_s(t,z) + M(t,z)\right) dt \tag{2}$$

where $P_s(t,z)$ is the rate of snow accumulation, $M(t,z)$ the rate of snow or ice melt (ablation) over the glacier's surface during the interval t_1 to t_2 (the hydrologic year). In practice Equation (2) is numerically integrated over a monthly time-scale to yield monthly melt that is then combined with available monthly precipitation data and then integrated over the hydrologic year.

Melt is determined using a melt (or degree-day) factor m_f that empirically relates ablation to mean daily air temperature $T_d(t,z)$:

$$M(z,t) = \begin{cases} m_f T_d(t,z) & T_d(t,z) > T_m \\ 0 & T_d(t,z) \le T_m \end{cases} \tag{3}$$

where T_m is a threshold temperature above which melting occurs.

The simplicity of the empirical approach to ice and snow ablation implicit in Equation (3) has the advantage of requiring far less meteorological data and/or parameterization than "enhanced" temperature-index models, or other energy balance approaches, wherein a radiation balance is considered. Furthermore, temperature-index methods perform well over basin-size spatial scales and intervals of time exceeding a few days (Hock, 1999; 2003). In recent comparisons of approaches to *long-term* ablation simulation, the performance of simple temperature-index methods compared favorably to, and in some instances exceeded, more physically-based models (e.g. Vincent and Six, 2013; Réveillet *et al*., 2017) or otherwise point to shortcomings of energy-balance models (Gabbi *et al.,* 2014). Thus TMs are especially suitable for determination of temperature depression during glaciation given the suite of meteorological and atmospheric unknowns.

Simulations were run using T_m = +1 °C but also 0 °C given both values have been used in previous studies (e.g. Hock, 1999; Pellicciotti *et al*. 2005; Gabbi *et al*., 2014; Réveillet *et al*., 2017;). Values m_f for snow and ice are taken as 0.45 and 0.80 cm water equivalent (w.e.) d^{-1} °C^{-1}, respectively as these are reasonable means of m_f values obtained for relatively debris-free ice and snow on modern glaciers (Hock, 2003; Braithwaite, 2008; Brugger, 2010). However, although there are outliers, m_f values for snow reported in the literature typically range from ~0.3 to ~0.6 cm w.e. d^{-1} °C^{-1}, while those for ice lie between ~0.6 and 1.0 cm w.e. d^{-1} °C^{-1}. Thus we show subsequently that our results are not unduly sensitive to the precise values of m_f. The latter is also significant in light of research that indicates degree-day factors vary spatially owing to local energy balances, for example topographic shading or surface slope and aspect, and temporally according to climate and weather (Hock, 2003; Pelliciotti *et al*., 2005; Mathews *et al*., 2015). In the TM the value of m_f is initially set for that of snow, but once snow melt exceeds accumulation it changes to that for ice.

In contrast to previous applications of the TM (Brugger, 2006; 2010) in which air temperature was assumed to vary sinusoidally about some annual mean, the algorithm used here is:

$$T_d(z,t) = \left[H \left[\frac{1-\cos\left(\left(\frac{2\pi d}{365}\right)-\phi\right)}{2} \right]^k - T_{jan}(z) \right] - \Delta T \qquad (4)$$

where H is the magnitude of the yearly temperature variation, d is the day of the year, ϕ is the phase lag (= 0.359 rads), and $T_{jan}(z)$ is the mean January temperature at elevation z, and ΔT is a prescribed perturbation of mean annual temperature (i.e. LGM temperature depression). Values of $T_{jan}(z)$ are calculated using modern lapse rates obtained using available data (Table 1) with respect to $T_{jan}(z)$ at a reference elevation. Table 1 also shows that a significant difference in the January lapse rate exists between the eastern and western sides of the Mosquito Range (also for other months) reflecting the difference in climates (which are also represented in the monthly PRISM models). Note that implementation of Equation (4) implies a uniform perturbation of temperature over the year, that is no temperature seasonality is examined in the present study. The constant k in Equation (4) is a tuning parameter that controls the sharpness of the temperature curve and allowed a better fit to observed temperatures. Values of k (1.46 on the east side of the range, 1.45 on the west) were chosen to minimize the root mean square error *RMSE* between simulated mean monthly temperatures and those recorded at all relevant meteorological stations. Particular attention was on accurately simulating temperatures during the ablation season (discussed subsequently). Values of H are remarkable consistent at all elevations on each side of the range (Table 1).

Snow accumulation $P_s(t,z)$ is determined by:

$$P_s(t,z) = fP_{mod}(t,z) + F \tag{5}$$

where $P_{mod}(t,z)$ is the modern precipitation, f is a partitioning function that determines what fraction of monthly precipitation fall as snow based on a continuous function of air temperature (Brugger, 2010), and F is a prescribed change in precipitation (i.e. assumed changes in precipitation during glaciation). Values for $P_{mod}(t,z)$ are calculated from the monthly fraction of the respective seasonal (winter, spring, summer, fall) totals and corresponding vertical precipitation gradients (Table 1). This approach is also a departure from previous implementations of the TM that used a vertical precipitation gradient based solely on mean annual precipitation. Use of seasonal gradients ensured that simulated precipitation, particularly that during the accumulation season (i.e. late fall to early spring), was not unduly influenced by the "steep" summer gradients that are significantly different and are poorly defined. It should be noted that summer, and more generally all, rain — not treated in temperature-index methods — can contribute to ablation but its contribution is usually negligible for non-maritime glaciers (Cuffey and Paterson, 2010). Monthly precipitation gradients for each season do not significantly differ (<10%) justifying the use of seasonal averages. The monthly fraction of seasonal precipitation is largely independent over the elevation range of interest here (~3000–4000m) with values varying less than ~10% during the accumulation season.

Results

Cosmogenic ^{10}Be exposure ages

Cosmogenic ^{10}Be exposure ages at Iowa Gulch (Table 3) yield distinct populations of ages across the two sampled moraine crests (Fig. 4). Two, zero-erosion exposure ages on the outer moraine are 115 ± 6 ka and 120 ± 5 ka, corresponding to the last global interglaciation during MIS 5e (Lisiecki and Raymo, 2005). The assumption of zero erosion at the boulder surface is inconsistent, however, with studies of exposed coarse-grained granitic rocks elsewhere in the Rocky Mountains (Benedict, 1993; Small *et al.*, 1997). Although it is not possible to precisely limit the rate of boulder surface erosion, Benedict (1993) estimated a time-averaged erosion rate of 1 mm kyr^{-1} at a similar altitude and latitude in Colorado. Applying that same erosion rate to surfaces IG-01-16 and IG-02-16 yields exposure ages of 133 ± 3 ka and 127 ± 4 ka. These ages align with the end of MIS 6, the time of the penultimate global glaciation. Cosmogenic ^{10}Be exposure ages of four boulders atop the inner moraine in Iowa Gulch yield a mean exposure age of 20.6 ± 1.1 ka (1σ). Three of the four exposure ages overlap at 1σ, with the fourth exposure (sample IG-04-16) being somewhat younger than the oldest three. We conclude that the mean of all four exposure ages represents the true age of the moraine, which is firmly within MIS 2.

In Union Canyon, four exposure ages (Table 3) from atop the recessional moraine (~1 km upvalley from the outermost Pinedale moraine; Fig. 4) feature three overlapping exposure ages with a mean of 17.1 ± 0.4 ka and one older exposure age (of 20.1 ± 0.5 ka) that does not overlap with the younger three at 2σ. The older exposure age is more consistent with the age of the terminal Pinedale moraine in Iowa Gulch, suggesting that ice in both valleys was at or near the maximum extent at ~20 ka. The younger three exposure ages in Union Canyon indicate that the ice was also near its maximum extent at 17.1 ± 0.4 ka.

Cosmogenic ^{10}Be exposure ages of Pinedale-age terminal and recessional moraines in the valleys of Twelvemile, Fourmile, and Sacramento Creeks (Table 3) are consistent with those at Iowa Gulch and Union Canyon, with a single exposure age from the terminal Pinedale moraine at Twelvemile Creek of 20.6 ± 0.5 ka and two exposure ages at Fourmile Creek with a mean of 21.7 ± 1.6 ka. One significantly older exposure age of the Fourmile Creek terminal moraine of 61.3 ± 0.6 ka and a slightly older age of 28.6 ± 1.0 ka on the Twelvemile Creek terminal moraine are interpreted as older outliers, possibly reworked boulders with ^{10}Be inventory from a period of prior exposure. A single younger exposure age from a recessional moraine in Fourmile Creek valley of 13.3 ± 0.2 ka is difficult to interpret without additional data, but may represent a late ice advance in the valley. The age of the only sample taken in the Sacramento Creek valley, 17.4 ± 1.3 ka, is consistent with those from the recessional moraine in Union Canyon.

Glacier Reconstructions

The geometries of the reconstructed glaciers (Fig. 2) are summarized in Table 2. Driving stresses tend to be low (~50 kPa) in the lower reaches of the reconstructed glaciers (Fig 2b). While not unreasonable, these most likely represent minimum values given underestimates of ice thickness due to post-LGM glacial and fluvial valley fill. Extrapolation of the bedrock walls of valley profiles suggests thicknesses (and therefore driving stresses) could have been as much 10-20% greater than estimated here. Additionally, in several valleys terminal moraine complexes are characterized by an abundance of ice disintegration/stagnation features that might also point to low driving stresses. Stresses of ~70 to 150 kPa are inferred for mid- and upper reaches of the reconstructed glaciers, the larger values being associated with steep surface slopes, associated with those of the underlying bedrock, and/or greater ice thickness.

Reconstructions indicate that glacier extent was greatest in the northern Mosquito Range, as noted previously, and that glaciers were larger on the eastern slope. A full explanation of this east-west asymmetry is beyond the scope of this work, but could certainly involve the land surface topography and possible precipitation differences during the last glaciation. An analysis of the hypsometry shows that the total land area above 3500 m, essentially corresponding to a rough average of equilibrium-line altitudes (ELAs, discussed subsequently), is almost 40% larger on the eastern side of the range (261 km^2 versus 191 km^2). While this analysis does not take into consideration slope angles, it nevertheless suggests a greater extent of areas of potential accumulation for glaciers on the east. Combined with the possibility of greater precipitation, total accumulation may have been significantly greater as well.

Temperature-index modeling: model verification

The robustness of the TM was evaluated by its ability to simulate modern climate and modern snowpack evolution at specific localities. It should be emphasized that local temperature and precipitation values are not explicitly used in the model, but rather determined from regional parameters. Figures 5a and b show that over the elevations most relevant to paleoglacier extents (~3000-4200 m), simulated temperatures agree quite well with those observed. Simulated temperatures during the ablation season are most critical because they drive melting. Temperatures during most of the accumulation season are less critical as these are well below the threshold for melting. Agreement during the ablation season is quantified by $RMSE_{abl}$ values that are less than 1 °C. Cumulative temperature differences over the ablation season $\Sigma\Delta_{abl}$ are also low, being less than ±0.5 °C. (Note that positive and negative values indicate the model respectively overestimates or underestimates a given quantity.) These values are representative of all other stations.

Similarly, the accuracy of modeled precipitation is more important during the accumulation season. Figures 5c and d (again typical of all stations in the appropriate elevation range) show that the model provides accurate representations of modern precipitation. Modeled values show less agreement with observations at Fremont Pass, however this station is somewhat outside the immediate study area. Climax, located two kilometers closer lies at essentially the same elevation yet receives ~8 cm (12%) less precipitation annually. Such spatial variability in precipitation is not uncommon (Anderton *et al*., 2004) and has been noted elsewhere in the region (Brugger, 2010). The Fremont Pass station notwithstanding, errors over the accumulation season ($RMSE_{acc}$) are < 1 cm for all stations between 3000 and 3500 m. Modeled precipitation on the east side of the Mosquito Range for the four stations of interest yield cumulative differences ($\Sigma\Delta_{acc}$) in precipitation of ~ ±2.5 cm for the accumulation season (Fig. 5d) On the western slope, $\Sigma\Delta_{acc}$ is between ±4.0 cm (three stations; data from the Leadville stations were averaged).

Perhaps the most stringent criteria to test the TM is how well it simulates modern snow accumulation and snowpack evolution (in w.e.) recorded in SNOTEL records (Figs. 5e and f) because this is most closely related to the goal of simulating glacier mass-balance. Simulations of the three SNOTEL records on the eastern side of the range are quite good with due consideration of, among others: (1) temporal differences in resolution (daily versus monthly in the model); (2) possible wind drifting or deflation of snow at observations sites (Meyer *et al*., 2012); (3) the effects of a tree canopy on local accumulation and ablation (Varhola *et al*., 2010). These factors can result in measured snow water equivalents at SNOTEL sites that are not representative of their surroundings (Molotch and Bales, 2005). Nevertheless, RMSE values (October-June/July) are less than 4.5 cm w.e. Because these reflect in part differences in temporal resolution, the differences (Δ_{snow}) in the maximum snow water equivalent might provide another metric of the ability of the TM to simulate snow accumulation. Δ_{snow} values ranged from –1.6 cm w.e. at the Rough and Tumble site to +4.1 cm w.e. at the Buckskin site (Fig 5f). Similar comparisons on the western slope of the Mosquito Range are problematic. Figure 5e shows that the model simulates less well the record at the Fremont Pass site (RMSE = 8.9 cm w.e., Δ_{snow} = –9.7 cm w.e.), the only SNOTEL on the west side of the range. However, this is an artifact of the inability of the model (and the inherent precipitation gradients used) to accurately simulate modern precipitation at this location as noted previously. Therefore, a “synthetic” record of snow accumulation at the Climax site was created by using cumulative (monthly) snow depths there and determining the mean density for late fall through early spring snowfall using data available for Fremont Pass. Agreement between the model and the synthetic record is better (RMSE = 3.0 cm w.e., Δ_{snow} = +7.9 cm w.e.), especially allowing for uncertainties in assumed snow density (Fig. 5e).

Varying m_f by ±0.2 cm w.e. d^{-1} °C^{-1} results in a change in maximum snowpack(s) by no more than ±3%. The only significant impact of this variation is to alter the length of time snow persists into the spring/summer (see for example the Hoosier Pass record in Fig. 6f). Changing the threshold temperature for melt (T_m in Equation (3)) to 0°C reduces maximum snowpack(s) by only a maximum of ~3% at all sites.

Temperature-index modeling: inferring Late Pleistocene glacial climate

Climate during the last glaciation is determined by finding the temperatures and/or precipitation that satisfy:

$$B_n = \int_A b_n dA \approx \sum_{i=1}^{j} b_{n_i} A_i = 0 \qquad (6)$$

where B_n is the steady-state mass-balance, A is glacier area composed of j number of discrete elevation intervals, and b_{n_i} is the mean annual specific net-balance over A_i. We emphasize that Equation (6) explicitly considers glacier hypsometry. However, solving Equation (6) presents the problem of equifinality, that is there are an infinite number of solutions that satisfy the condition $B_n = 0$. Therefore, reasonable limits must be imposed on assumed temperature-precipitation combinations.

With regard to the foregoing, the most straightforward assumption is that precipitation during the last glaciation was comparable to that today (i.e. $F = 0$ (Equation (5)). Under this assumption, simulations suggest temperature depressions between 7.9 and 8.2 °C are required to maintain steady-state mass balances of glaciers on the east side and between 7.4 and 7.7 °C on the west side of the Mosquito Range (Table 4). The respective averages are 8.1 ± 0.3 °C and 7.5 ± 0.2 °C. Uncertainties for individual estimates of temperature depression were +0.8 and –0.9 °C based on sensitivity analysis of the TI model (see Supporting Information for a complete analysis).

The associated ELAs are consistently lower on the east than on the west side of the range, averaging ~3485 ± 30 m and 3575 ± 25 m respectively. Average ELAs determined using the accumulation-area ratio method (AAR = 0.65) are lower than their simulated counterparts by ~10 to 45 m but show a similar consistency (Table 4). Lower ELAs on the east side of the range might also suggest that differences between precipitation on the eastern and western slopes of the Mosquito Range similar to those today existed during the last glaciation. This is discussed further in a subsequent section.

Whether precipitation during the last glaciation differed from that of today is more challenging to assess because the Colorado Rocky Mountain region lacks paleoclimate proxies that might constrain precipitation. Moreover, despite their resolution, global and regional climate simulations of the last glaciation from model ensembles suggest only slight changes in precipitation in this region and are equivocal whether climate was wetter or drier (e.g. Braconnot *et al*. 2007; Oster *et al*., 2015; Lora *et al*., 2017). Differences in precipitation are also indicated by climate reconstructions using pollen-based proxies (Izumi and Bartlein, 2016). Thus it is prudent to consider scenarios in which the last glaciation in the Mosquito Range was wetter or drier.

Figure 6 shows the effect of potential changes in precipitation on the temperature depression required for steady-state glacier mass-balances. Not surprisingly, greater/smaller temperature depression (i.e. less/more ablation) must be offset by concomitant reductions/increase in precipitation (less accumulation). Given the magnitudes suggested by paleoclimate reconstructions for western North America (Kim *et al*., 2008; Ibarra *et al*., 2014; Oster *et al*., 2015; Lora *et al*., 2017), we allow annual precipitation to vary slightly by ± 10 cm. Changes of this magnitude are ±15-25% of modern MAP values (depending on location and elevation) and therefore might be considered too great. Table 4 and Figure 6 show that under slightly wetter conditions the required temperature depressions are 7.5 ± 0.3 °C for the eastern side and 7.0 ± 0.2 °C for the western side of the range. If the last glacial climate was slightly drier, the corresponding temperature depressions are 8.9 ± 0.3 and 8.0 ± 0.2 °C respectively. Assuming arguably extreme changes in precipitation, say +50 cm and –20 cm — not supported by any studies of which we are aware — the required temperature depressions might have been between ~5.6 and 9.9 °C (Fig. 6). (Note that reductions in precipitation by more than 20 cm are precluded as this results in no precipitation at lower elevations.)

Discussion

Chronology of glacial deposits

On the Bull Lake moraine segment in Iowa Gulch, the mean of two ^{10}Be ages is 130 ± 5 ka after allowing for a reasonable rate of rock erosion (1 mm kyr^{-1}). Schweinsberg *et al*. (2017), using the same erosion rate and a similar cosmogenic-isotope production scaling model, obtained a mean age of 132 ± 8 ka for four boulders on a Bull Lake-aged moraine fronting the Lake Creek Valley on the eastern side of the Sawatch Range (TL on Fig. 1b). Unfortunately, there are few other exposure ages for comparably-aged moraines elsewhere in Colorado. Benson *et al*. (2004) found anomalously young ^{36}Cl ages on four of five Bull Lake boulders in the Park and Front Ranges that were attributed to combination of erosion, snow and sediment shielding, and ^{36}Cl leakage. The fifth yielded a zero-erosion, shielding uncorrected age of ~144 ka (original value). Dethier *et al*. (2000) reported *minimum* mean ^{10}Be and ^{26}Al ages of 101 ± 21 ka and 122 ± 26 ka (original values) on Bull Lake moraines in the Front Range. Schildgen at al. (2002) dated an associated Bull Lake terrace at 133 ± 28 ^{10}Be ka and 139 ± 31 ^{26}Al ka (original values). The younger minimum ages notwithstanding, these age estimates are in good agreement and indicate broad regional synchrony of glacial advances during MIS 6.

Exposure ages obtained on Pinedale-age (MIS 2) terminal moraines in the Mosquito Range (Table 3) span an interval from 22.8 ± 0.2 to 19.0 ± 0.6 ka. Five overlapping ages (Fig. 7a) yield a mean age of 20.9 ± 0.4 ka. Alternatively, inclusion of the oldest and youngest ages yields an identical mean age of 20.9 ± 1.1 ka. The probability density plot shows a dominant peak at 20.6 ka. Several authors (e.g. Applegate *et al*., 2010; Heyman *et al*., 2011; Leonard *et al*., 2017b) have pointed out that the ages (mean, distribution, and so forth) of moraine boulders can be interpreted differently. We follow Leonard *et al*. (2017b) and numerous other studies by using the mean exposure age to indicate the timing of moraine abandonment following the maximum ice extent, while at the same time providing a minimum age for the Pinedale maximum. Thus we argue that the last glaciation in the Mosquito Range culminated at ~20–21 ka during the latter part of the global Last Glacial Maximum (26.5 to 19.0 ka; Clark *et al*., 2009). This timing is consistent with the conclusions of a recent review of available cosmogenic exposure ages in Colorado by Leonard *et al*. (2017b) wherein they showed that individual valley glacier maxima generally occurred prior to ~19.5 ka.

Leonard *et al*. (2017b) also concluded that retreat or abandonment of terminal moraines in Colorado was asynchronous, possibly well underway at ~17–16 ka in the San Juan Mountains and Front Range, while glaciers remained at or near their maximum extents in the Sawatch Range and Sangre de Cristo Mountains at that time. The younger ^{10}Be ages on the recessional moraine in Union Canyon (Fig. 4) suggest that, at least in this valley, glaciers were close to their maximum extent at ~17 ka suggesting a similar early deglaciation history in the Mosquito Range as those in the immediately adjacent ranges. This apparent asynchronous response across the region begs the question as to what climatic conditions and/or dynamic factors allowed glaciers to persist at or nearly maximum extents in some glacial valleys and not others. Asynchronous glacier maxima in the Sawatch Range was reported by Young *et al*. (2011), who suggest that differences in glacier shape, aspect, and hypsometry may have resulted in temporal differences in valley glacier advance and retreat during the last glaciation. It is worth noting, however, that more extensive ice in the Sawatch Range, the Sangre de Cristo Mountains and Mosquito Range at ~17 ka is coeval with glacier maxima and/or readvances documented in other glaciated ranges in the U.S. Rocky Mountains as further discussed below.

Glacial chronology and regional climate

The Pinedale maximum in the Mosquito Range at 21–20 ka was coincident with an insolation minimum (Fig. 7g) and cooler Northern Hemispheric temperatures (Fig. 7b). It corresponded to the global LGM (Clark *et al*., 2009; Lisiecki and Raymo, 2005), the time when southern outlets of the Laurentide Ice Sheet were at their maximum extent (Ullman *et al*., 2015), and with mountain glacier maxima elsewhere in the Rocky Mountains of Utah (Laabs *et al*., 2009; Quirk *et al*., 2018) and Wyoming (Dahms *et al*., 2018). This time interval also featured wetter and/or cooler winters reflected in speleothem records from the southwestern U.S. (Fig. 7d-f). Paleohydrologic studies (Ibarra *et al*., 2014; 2018) indicate minimal increases in LGM precipitation in the northern Great Basin (at latitudes greater than the Mosquito Range) but much greater increases at latitude similar to the Mosquito Range, suggesting the latter proxies may reflect precipitation increases during the Pinedale Maximum.

Extensive ice at 17 ka is coeval with glacier maxima in the nearby Sangre de Christo Range (Leonard *et al*., 2017a) and Sawatch Range (Young *et al*., 2011; Schweinsberg *et al*., 2016) and with glacier readvances to near maximum lengths in the Wasatch and Uinta Ranges of the Middle Rocky Mountains (Laabs and Munroe, 2016; Quirk *et al*., 2018), and maximum extents of several outlet glaciers of the Greater Yellowstone Glacial System (Licciardi and Pierce, 2008, 2018; their “middle Pinedale). The potential driver of glacier readvance or persistence near their maximum lengths may be related to regional precipitation changes following the LGM (e.g., Thackray *et al*., 2004; Thackray, 2008). This is consistent with the observed highstands of many of the pluvial lakes in the Southwestern U.S. at 17-16 ka (Fig. 7c; Munroe and Laabs, 2013), coeval wetter and/or cooler conditions as revealed by speleothem records (Fig.

7d-f; Wagner *et al*., 2010; Asmerom *et al*., 2010; Moseley *et al*., 2016) and reconstructed lake highstands (Lyle *et al*., 2012; Ibarra *et al*., 2014; 2018) following the initial phase of deglaciation. The timing of these events falls within the Heinrich Stadial 1 (ca. 18-15 ka; Figs. 7 and 8) that is associated with a hemispheric cooling owing to a weakening of the Atlantic Meridional Overturning Circulation (McManus *et al*., 2004). However, regional asynchrony of deglaciation and in the highstands of some pluvial lakes (Munroe and Laabs, 2013; Ibarra *et al*., 2014) implies a degree of local modulation of hemispheric climate forcing(s).

Last glacial climate in the Mosquito Range

Our results suggest that in the absence of any changes in precipitation, temperatures in the Mosquito Range were between 7.5 and 8.1 °C cooler during the Pinedale maximum compared to modern. Considering the uncertainty (+0.8/–0.9°C), these values agree and one could conclude there was no significant difference in temperature depression with respect to the eastern and western slopes. In detail, however, the difference is largely an artifact of those in modern, and presumed last glacial precipitation. This begs the question as to whether temperature depression could have differed over the range. A reasonable assumption is that regional temperature was more uniform than precipitation. If an average glacial temperature depression of 7.8 °C for the whole of the Mosquito Range is assumed, a precipitation increase of ~5 cm over modern is required on the eastern side of the range while a decrease of similar magnitude is required on the western side (Fig. 6). This outcome therefore suggests that the difference in precipitation across the range observed today was somewhat accentuated during the last glaciation.

Independent estimates of ELAs based on the AAR method (Table 4) that are consistently lower on the eastern side of the range compared to the western side might also point to differences in precipitation. Refsnider *et al*. (2009) noted a similar cross-range difference in ELAs in the Sangre de Cristo Mountains ~100 km to the south. They attributed this to an enhancement of late winter/early spring southeasterly-derived (Gulf of Mexico) moisture that would have preferentially nourished glaciers on the eastern slopes. We offer this as a viable explanation for the *apparent* east-west differences in Late Pleistocene glacial temperature depression obtained by our simulations. This conclusion is consistent with the fact that modern winter precipitation – presumably therefore snow accumulation – is greater on the eastern slopes of the Mosquito Range due to late winter/early spring events.

Interestingly, a high-resolution paleoclimate simulation for North America (Kim *et al*., 2008; their Fig. 8) indicates a sharp east-west gradient in LGM winter precipitation (December-February in their study) in the general region of the study area. Their simulation suggests that this gradient arises by a combination of increases over modern precipitation in the east and decreases in the west, and by magnitudes greater than those implied by our simulations. Thus our conclusion that the present difference in winter precipitation across the Mosquito Range not only existed during the last glaciation, but was could have been more pronounced, is not unreasonable. Moreover, *if* the North American summer monsoon strengthened (*cf*. Lachniet *et al*., 2013; Bhattachary *et al*., 2017), then greater increases in precipitation on the eastern slopes that would fall as snow at higher elevations, would have further increased accumulation differences across the range.

Our average estimate of glacial temperature depression of 7.8 +0.8/–0.9 °C in the Mosquito Range compares favorably with estimates elsewhere in the Colorado Rocky Mountains (Table 5). (Unless, otherwise indicated, subsequent comparisons assume no significant changes in precipitation.) Brugger (2010), using a slight variation of the TM used in the present study, found MATs were on average 6.9 ± 0.6 °C cooler for the southern Sawatch Range and Elk Mountains to the west. In the same area, Brugger and Goldstein (1999) suggested a temperature depression of 7.0–9.0 °C based on climatic interpretation of lowered ELAs. Preliminary TM simulations (Brugger *et al*., 2017) suggests a LGM temperature depression of ~6.2 and ~7.5 °C to maintain glaciers in the northern Sawatch Range, immediately to the west of the study area. Refsnider *et al*. (2009) concluded that mean summer temperatures in the Sangre de Cristo Mountains in southern Colorado were ~6.0–7.5 °C cooler, varying according to assumed changes in precipitation. In a sub-region of those same mountains, the Blanca Massif, Brugger *et al*. (2009) suggested 7.0–8.0 °C of cooling based on TM simulations. In contrast, Leonard *et al*., (2017a) using a coupled energy-mass balance-flow model, determined that LGM temperatures were ~5.0 +1.5/–1.0 °C cooler in the Sangre de Cristo Mountains. Leonard and Russell (in Schweinsberg, *et al*., 2016) applied the same approach and determined temperatures were depressed 5.4 °C in the northern Sawatch. Dühnforth and Anderson (2011), who employed a numerical model of glacier flow with parameterized mass-balance components, found that temperatures were between 4.5 and 5.8 °C cooler in Front Range, farther afield to the northeast. In a broader regional study based on climate at equilibrium-lines, Leonard (1989) concluded temperatures in Colorado were ~8.5 °C cooler. Leonard (2007) later used this approach within a GIS-based model and concluded that Late Pleistocene glaciers in central Colorado would have required an average temperature depression of 7.6 ± 0.7 °C.

The relatively small disparities in estimates of last glacial temperature depression are undoubtedly due in part to differences in the methodologies used, and they are perhaps smaller than they first appear when considering the associated uncertainties (when reported). There are, however, other potential explanations that might either wholly or partially reconcile these differences. First, LGM temperature depression during the Pinedale maximum might have indeed vary throughout the region; that is, an *a priori* assumption that regional temperature (and precipitation) change during the Pinedale was uniform and not modulated by local, or microclimatic influences is questionable. Climate simulations of the LGM indicate changes in MATs in the specific geographic areas referenced above were between ~ –8.0 and –

10.0 °C (e.g. Paleoclimate Modeling Intercomparison Project 3 ensemble means, Oster *et al.*, 2015, Supplementary Table S-9; Community Climate System Model (CCSM) 3, Lorenz *et al.*, 2016; CCSM4, data available at WorldClim - Global Climate Data, http://www.worldclim.org). While these results appear to corroborate the idea that temperature change during the Pinedale maximum might have varied somewhat, the stated 1σ ~ ±2.9 °C associated with these means precludes any definite conclusion.

The foregoing methodologies also depend on the extents of paleoglaciers delineated by terminal moraines and their precise relationship with regional climate. Addition complications in directly comparing derived temperature depression can be therefore introduced by virtue of potential ambiguities in the relationships among/between climate forcing(s), glacier response, and interpretations of moraine ages (Kirkbride and Winkler, 2012). A full discussion of these is beyond the scope of this study, rather they are outlined here in order to provide a context for comparing the timing and magnitude of glacial cooling in the Colorado Rocky Mountains. In short, the Pinedale maximum (used here in the strict sense of the timing of maximum downvalley glacier extent) might have been time-transgressive (Young *et al.*, 2011) and spatially variable owing to (1) microclimates modulating regional/global climate differently so local forcings were asynchronous; (2) differences in valley glacier response times (e.g. Pelto and Hedlund, 2001; Brugger, 2007a) related to glacier hypsometries, (Young *et al.*, 2011; Chenet *et al.*, 2010) or valley topography (Pratt-Sitaula *et al.*, 2011) that led to asynchronous behavior; and/or (3) maximum glacier extent is not indicative of the mean glacial climate but rather a reflection of a single, transient response(s) to stochastic interannual variations in temperature (Anderson *et al.*, 2014). Therefore, attaching inordinate significance to *minor* differences in estimates of LGM temperature depression should perhaps be avoided.

Conclusions

Moraine boulder ^{10}Be surface exposure ages in four valleys in the Mosquito Range reveal that terminal moraine deposition occurred during MIS 6 and MIS 2. During the Pinedale Glaciation, valley glaciers were at or near their maximum extents ~21–20 ka. Exposure ages of boulders on a recessional moraine suggest that ice retreat was under way by ~17 ka. Temperature-index modeling suggests that during the Pinedale maximum, steady-state mass balances of glaciers on the east side of the range required temperatures that were on average 8.1 °C less than modern, assuming no change(s) in precipitation. Glaciers on the west side of the range existed under temperatures 7.5 °C cooler. Given uncertainties of +0.8/–0.9 °C, a glacial temperature depression of 7.8 °C is implied. Under the assumption that temperature depression was uniform over the Mosquito Range, precipitation differences that exist today across the range might have been enhanced during the last glaciation, potentially by strengthening of the

North American summer monsoon. If precipitation increased or decrease slightly (± 10 cm) as suggested by some climate reconstructions, temperature depression could have been between 7.0 and 8.9 °C.

Within the bounds of uncertainties, the new chronology for the last glaciation in the Mosquito Range presented here is in good agreement with those developed for the northern Sawatch Range and Elk Mountains, the Front Range, the Sangre de Cristo Mountains, and the San Juan Mountains. The timing of the LGM in the Colorado Rocky Mountains thus appears to have been broadly synchronous and driven by regional cooling and perhaps slight enhancements in winter precipitation. In contrast, initial deglaciation was asynchronous, beginning first in the Front Range and San Juan Mountains and later in the Mosquito Range, Sawatch Range, and Sangre de Cristo Mountains.

Our estimate(s) of temperature change in the Mosquito Range during the Pinedale maximum is also consistent with those similarly-derived for other mountain ranges in Colorado and with those based on climate at ELAs. Furthermore, it is consistent with temperature depressions inferred from regional-scale modeling of LGM paleoclimate. Differences exist, however, between our estimate and those based on coupled glacier flow-mass-balance models that yield temperature depressions on the order of 5–6 °C. These differences, while possibly real, are small considering the associated quantifiable uncertainties in the approaches used *combined with* the possibility of spatially varying changes in LGM precipitation.

Supporting Information

Text. Processing of moraine boulder samples and calculation of ^{10}Be exposure ages, and modeling uncertainties.

Table S1. Cosmogenic ^{10}Be sample data and exposure ages.

Table S2. Sensitivity analysis of the TI model and resulting uncertainties.

Acknowledgements

Funding for initial cosmogenic dating and fieldwork was provided to KAB by the UMM's Faculty Research Enhancement Funds. A seed grant to KAB and BL from the Purdue University PRIME Lab provided AMS analyses of additional samples. NB was supported by the University of Minnesota's Undergraduate Research Opportunity Program. BL and AR gratefully acknowledge support of the NDSU College of Science and Math. We also thank the reviewers for their thorough and thoughtful comments.

References

Asmerom, Y., Polyak, V.J., Burns, S.J., 2010. Variable winter moisture in the southwestern United States linked to rapid glacial climate shifts. Nat. Geosci. 3, 114**e**117.

Anderson LS, Roe GH, Anderson RS. 2014. The effects of interannual climate variability on the moraine record. *Geology* **42**: 55-58.

Anderton SP, White SM, Alvera B. 2004. Evaluation of spatial variability in snow water equivalent for a high mountain catchment. *Hydrologic Processes* **18**: 435–453.

Applegate PJ, Urban NM, Laabs BJC, *et al*. 2010. Modeling the statistical distributions of cosmogenic exposure dates from moraines. *Geoscientific Model Development* **3**: 293-307.

Benedict JB. 1993. Influence of snow upon rates of granodiorites weathering, Colorado Front Range USA. *Boreas* **22**: 87–92.

Benson L, Madole R, Phillips *et al*. 2004. The probable importance of snow and sediment shielding on cosmogenic ages of north-central Colorado Pinedale and pre-Pinedale moraines. *Quaternary Science Reviews* **23**: 193-206.

Berger, A. 1992. Orbital variations and insolation database. IGBP PAGES/World Data Center for Paleoclimatology, Data Contribution Series 92-007, NOAA/NGDC Paleoclimate Program , Boulder Colorado, USA.

Bhattacharya T, Tierney JE, DiNezio P. 2017. Glacial reduction of the North American Monsoon via surface cooling and atmospheric ventilation. *Geophysical Research Letters* **44**: 5113–5122.

Bindschadler R, Harrison WD, Raymond CF *et al*. 1977. Geometry and dynamics of a surge-type glacier. *Journal of Glaciology* **18**: 181-194.

Bohannon RG, Ruleman CA. 2013. Geologic map of the Mount Sherman 7.5’ Quadrangle, Lake and Park Counties, Colorado. United States Geologic Survey Scientific Investigation Map 3271.

Braconnot P, Otto-Bliesner B, Harrison S *et al*. 2007. Results of PMIP2 coupled simulations of the Mid-Holocene and Last Glacial Maximum – Part 1: experiments and large-scale features. *Climates of the Past* **3**: 261-277.

Braconnot P, Harrison SP, Kageyama M *et al*. 2012. Evaluation of climate models using paleoclimatic data. *Nature Climate Change* **2**: 417-424.

Braithwaite, RJ. 2008. Temperature and precipitation climate at the equilibrium-line altitude of glaciers expressed by the degree-day factor for melting snow. *Journal of Glaciology* **54**: 437-444.

Brugger KA. 2006. Late Pleistocene climate inferred from the reconstruction of the Taylor River Glacier Complex, southern Sawatch Range, Colorado. *Geomorphology* **75**: 318-329.

Brugger KA. 2007a. The non-synchronous response of Rabots Glaciär and Storglaciären to recent climate change: a comparative study. *Annals of Glaciology* **46**: 275-282.

Brugger KA. 2010. Climate in the southern Sawatch Range and Elk Mountains, Colorado, USA, during the Last Glacial Maximum: inferences using a simple degree-day model. *Arctic, Antarctic, and Alpine Research* **42**: 164-178.

Brugger KA, Goldstein BS. 1999. Paleoglacier reconstruction and late-Pleistocene equilibrium-line altitudes, southern Sawatch Range, Colorado. In *Glacial Processes Past and Present*, Mickelson DM, Attig JW (eds.), Geological Society of America Special Paper 337; 103–112.

Brugger KA., Refsnider KA, Leonard, EM. 2009. Late Pleistocene climate on the Blanca Massif, Sangre de Cristo Range, Colorado. *Geological Society of America Abstracts with Programs* **41**: 640.

Brugger KA, Ruleman CA, Caffee MW. 2017. Glaciation and climate during the Last Glacial Maximum in the Mount Massive region, northern Sawatch Range, Colorado. *Geological Society of America Abstracts with Programs* **49**: 6.

Chenet M, Roussel E, Jomelli V *et al*. 2010. Asynchronous Little Ice Age glacial maximum extent in southeast Iceland. *Geomorphology* 114: 253-260.

Clark PU, Dyke AS, Shakun JD *et al*. 2009. The last glacial maximum. *Science* **325**: 710-714.

Cuffey KM, Paterson WSB. 2010. *The Physics of Glaciers (4th ed.)*. Elsevier, Boston.

Dahms D, Egli M, Fabel D *et al*. 2018. Revised Quaternary glacial succession and post-LGM recession, southern Wind River Range, Wyoming, USA. *Quaternary Science Reviews* **192**: 167-184.

Dethier DP, Schildgen TF, Bierman P *et al*. 2000. The cosmogenic isotope record of late Pleistocene incision, Boulder Canyon, Colorado. *Geological Society of America Abstracts with Programs* **32**: 473.

Dühnforth M, Anderson RS. 2011. Reconstructing the glacial history of green lakes valley, North Boulder Creek, Colorado Front Range. *Arctic, Antarctic, and Alpine Research*. **43:** 527-542.

Flato G, Marotzke J, Abiodun B *et al*. 2013. Evaluation of climate models. In *Climate Change 2013: The Physical Science Basis. Contribution of Working Group I to the Fifth Assessment Report of the Intergovernmental Panel on Climate Change*. Stocker, TF, Qin D, Plattner GK, *et al*. (eds). Cambridge University Press, Cambridge and New York; 741-866.

Gabbi J, Carenzo M, Pellicciotto F *et al*. 2014. A comparison of empirical and physically based glacier surface melt models for long-term simulation of glacier response. *Journal of Glaciology* **60**: 1140-1154.

Gosse JC, Klein J, Lawn B et al., 1995. Beryllium-10 dating of the duration and retreat of the last Pinedale glacial sequence. *Science* **268**: 1329-1333.

Higgins RW, Yao Y, Wang XL. 1997. Influence of the North American Monsoon system on the U.S. summer precipitation regime. *Journal of Climate* **10**: 2600-2622.

Hock R. 1999. A distributed temperature-index ice- and snowmelt model including potential direct solar radiation. *Journal of Glaciology* **45**: 101–111.

Hock R. 2003. Temperature index melt modelling in mountain areas. *Journal of Hydrology* **282**: 104–115.

Heyman J, Stroeven AP, Harbor JM *et al*. 2011. Too young or too old: evaluating cosmogenic exposure dating based in an analysis of compiled boulder ages. *Earth and Planetary Science Letters* **302**: 71-80.

Ibarra DE, Egger AE, Weaver KL, *et al*. 2014. Rise and fall of late Pleistocene pluvial lakes in response to reduced evaporation and precipitation: evidence from Lake Surprise, California. *Geological Society of American Bulletin* **126**: 1387-1415.

Ibarra DE, Oster JL, Winnick, MJ *et al*. 2018. Warm and cold wet states in the western United States during the Pliocene–Pleistocene. *Geology* **46**: 355-358.

Izumi K, Bartlein, PJ. 2016. North American paleoclimate reconstructions for the Last Glacial Maximum using an inverse modeling through iterative forward modeling approach applied to pollen data, *Geophysical Research Letters* **43**: 10,965**–**10,972.

Kageyama M, Albani S, Braconnot et al. 2017. The PMIP4 contribution to CMIP6 - Part 4: scientific objectives and experimental design of the PMIP4-CMIP6 last glacial maximum experiments and PMIP4 sensitivity experiments. *Geoscientific Model Development* **10**: 4035-4055.

Kellogg KS, Shroba RR, Ruleman CA *et al*. 2017. Geologic map of the Upper Arkansas River Valley region, north-central Colorado. United States Geologic Survey Scientific Investigation Map 3382.

Kim S-J, Crowley TJ, Erickson DJ, *et al*. 2008. High-resolution climate simulation of the last glacial maximum. *Climate Dynamics* **31**: 1-16.

Kirkbride MP, Winkler S. 2012. Correlation of Late Quaternary moraines: impact of climate variability, glacier response, and chronological resolution. *Quaternary Science Reviews* **46:** 1–29.

Laabs BJC, Munroe JS. 2016. Late Pleistocene mountain glaciation in the Lake Bonneville basin. In *Developments in Earth Surface Processes* **20**: 462-503.

Laabs BJ, Refsnider KA, Munroe JS *et al*. 2009. Latest Pleistocene glacial chronology of the Uinta Mountains: support for moisture-driven asynchrony of the last deglaciation. *Quaternary Science Reviews* **28**: 1171-1187.

Lachniet MS, Asmerom Y, Bernal JP *et al*. 2013. Orbital pacing and ocean circulation-induced collapses of the Mesoamerican monsoon over the past 22,000 y. *Proceedings of the National Academy of Sciences* **110**: 9255-9260.

Leonard EM. 1989. Climatic change in the Colorado Rocky Mountains: estimates based on modern climate at late Pleistocene equilibrium lines: *Arctic and Alpine Research* **21:** 245-255.

Leonard EM. 2007. Modeled patterns of Late Pleistocene glacier inception and growth in the Southern and Central Rocky Mountains, USA: sensitivity to climate change and paleoclimatic implications. *Quaternary Science Reviews* **26**: 2152-2166.

Leonard EM, Laabs BJC, Plummer MA *et al*. 2017a. Late Pleistocene glaciation and deglaciation in the Crestone Peaks area, Sangre de Cristo Mountains, USA - chronology and paleoclimate. *Quaternary Science Reviews* **158:** 127-144.

Leonard EM, Laabs BJC, Schweinsberg *et al*. 2017b. Deglaciation of the Colorado Rocky Mountains following the Last Glacial Maximum. Cuadernos de Investigación Geográfica 43: 497-526.

Licciardi JM, Clark PU, Brook EJ *et al*. 2001. Cosmogenic ^{3}He and ^{10}Be chronologies of the late Pinedale northern Yellowstone ice cap, Montana, USA. *Geology* **29**: 1095–1098.

Licciardi JM, Clark PU, Brook EJ *et al*. 2004. Variable responses of western U.S. glaciers during the last deglaciation. *Geology* **32**: 81–84.

Licciardi JM, Pierce KL. 2008. Cosmogenic exposure-age chronologies of Pinedale and Bull Lake glaciations in greater Yellowstone and the Teton Range, USA. *Quaternary Science Reviews* **27**: 814-831.

Licciardi JM, Pierce KL. 2018. History and dynamics of the Greater Yellowstone Glacial System during the last two glaciations. *Quaternary Science Reviews* **200:** 1-33.

Lisiecki LE, Raymo ME. 2005. A Pliocene-Pleistocene stack of 57 globally distributed benthic δ18O records. *Paleoceanography* **20**: PA1003.

Lora JM, Mitchell JL, Risi C *et al*. 2017. North Pacific atmospheric rivers and their influence on western North America at the Last Glacial Maximum. *Geophysical Research Letters* **44**, 1051–1059.

Lorenz DJ, Nieto-Lugilde D, Blois JL *et al*. 2016. Downscaled and debiased climate simulations for North America from 21,000 years ago to 2100 AD. *Scientific Data* **3**.

Lyle M, Heusser L, Ravelo C *et al*. 2012. Out of the Tropics: The Pacific, Great Basin Lakes, and the late Pleistocene water cycle in the western United States. *Science* **337**: 1629-1633.

Matthews T, Hodgkins R, Wilby RL *et al*. 2015. Conditioning temperature-index model parameters on synoptic weather types for glacier melt simulations. *Hydrologic Processes* **29**: 1027-1045.

McCalpin JP, Funk J, Mendel D. 2012. Leadville South Quadrangle Geologic Map, Lake County, Colorado. Colorado Geological Survey, Denver, Colorado.

McCalpin JP, Temple J, Sicard K *et al*. 2012. Climax Quadrangle Geologic Map, Lake and Park Counties, Colorado. Colorado Geological Survey, Denver, Colorado.

McManus JF, Francois R, Gherardi J-M *et al*. 2004. Collapse and rapid resumption of the Atlantic meridional circulation linked to deglacial climate changes. *Nature* **428**: 834-837.

Meyer JDD, Jin J, Wang S-Y. 2012. Systematic patterns of the inconsistency between snow water equivalent and accumulation precipitation as reported by the snowpack telemetry network. *Journal of Hydrometeorology* **13**: 1970-1976.

Molotch NP, Bales RC. 2005. Scaling snow observations from the point to the grid element: Implications for observation network design. *Water Resources Research* **41**: W11421

Moseley GE, Edwards RL, Wendt KA *et al*. 2016. Reconciliation of the Devils Hole climate record with orbital forcing. *Science* **351**: 165-168.

Munroe JS, Laabs BJC. 2013. Temporal correspondence between pluvial lake highstands in the southwestern US and Heinrich Event 1. *Journal of Quaternary Science* **28**: 49-58.

Nye JF. 1965. The flow of a glacier in a channel of rectangular, elliptic or parabolic cross-section. *Journal of Glaciology*, **5**: 661-690.

Oster JL, Ibarra DE, Winnick, MJ *et al*. 2015. Steering of westerly storms over western North America at the Last Glacial Maximum. *Nature Geoscience* **8:** 201-205.

Pellicciotti F, Brock B, Strasser U *et al*. 2005. An enhanced temperature-index glacier melt model including a shortwave radiation balance: development and testing for Haut Glacier d'Arolla, Switzerland. *Journal of Glaciology* **175**: 573-587.

Pelto MS, Hedlund C. 2001. Terminus behavior and response time of North Cascade glaciers, Washington, USA. *Journal of Glaciology*, **47**: 497-506.

Phillips FM, Zreda MG, Smith SS *et al*. 1990. Cosmogenic chlorine-36 chronology for glacial deposits at Bloody Canyon, eastern Sierra Nevada. *Science* **248**: 1529-1532.

Phillips FM, Zreda MG, Benson LV *et al*. 1996. Chronology of fluctuations in late Pleistocene Sierra Nevada glaciers and lakes. *Science* **274**: 749-751.

Phillips FM, Zreda MG, Plummer MA *et al*. 2009. Glacial geology and chronology of Bishop Creek and vicinity, ester Sierra Nevada, California. *Geological Society of American Bulletin* **121**: 1013-1033.

Pratt-Sitaula B, Burbank DW, Heimsath AM *et al*. 2011. Topographic control of asynchronous glacier advances: a case study from Annapurna, Nepal. *Geophysical Research Letters* **38**: L24502.

Quirk BJ, Moore JR, Laabs BJ *et al*. 2018. Termination II, Last Glacial Maximum, and Late glacial chronologies and paleoclimate from Big Cottonwood Canyon, Wasatch Mountains, Utah. *Geological Society of America Bulletin* **130**: 1889-1902.

Rasmussen S O, Andersen KK, Svensson AM *et al*. 2006. A new Greenland ice core chronology for the last glacial termination. *Journal of Geophysical Research: Atmospheres* **111**: D06102.

Refsnider KA, Brugger KA, Leonard EM *et al*. 2009. Last glacial maximum equilibrium-line altitude trends and precipitation patterns in the Sangre de Cristo Mountains, southern Colorado, USA. *Boreas* **38:** 663-678.

Réveillet M, Vincent C, Six D, Rabatel A. 2017. Which empirical model is best suited to simulate glacier mass balances? *Journal of Glaciology* **63**: 39-54.

Schildgen T, Dethier DP, Bierman P *et al*. 2002. ^{26}Al and ^{10}Be dating of late Pleistocene and Holocene fill terraces: a record of fluvial deposition and incision, Colorado Front Range. *Earth Surface Processes and Landforms* **27**: 773-787.

Schweinsberg AD, Briner, JP, Shroba, RR *et al*. 2016. Pinedale glacial history of the upper Arkansas River valley: new moraine chronologies, modeling results, and geologic mapping. In Keller SM, Morgan ML (eds.) Unfolding the Geology of the West: Geological Society of America Field Guide, 44; 335-353.

Small EE, Anderson RS, Repka JL *et al*. 1997. Erosion rates of alpine bedrock summit surfaces deduced from in situ ^{10}Be and ^{26}Al. *Earth and Planetary Science Letters* **150**: 413-425.

Thackray GD, Lundeen KA, Borgert JA. 2004. Latest Pleistocene alpine glacier advances in the Sawtooth Mountains, Idaho, USA: reflections of midlatitude moisture transport at the close of the last glaciation. *Geology* **32**: 225-228.

Thackray, GD 2008. Varied climatic and topographic influences on Late Pleistocene mountain glaciation in the western United States. *Journal of Quaternary Science* **23**: 671-681.

Ullman DJ, Carlson AE, LeGrande AN *et al*. 2015. Southern Laurentide ice-sheet retreat synchronous with rising boreal summer insolation. *Geology* **43**: 23-26.

Varhola A, Coops NC, Weiler M *et al*. 2010. Forest canopy effects on snow accumulation and ablation: an integrative review of empirical results. *Journal of Hydrology* **392**: 219-233.

Vincent C, Six D. 2013. Relative contribution of solar radiation and temperature in enhanced temperature-index melt models from a case study at Glacier de Saint-Sorlin, France. *Annals of Glaciology* **54**: 11-17.

Wagner JD, Cole JE, Beck JW *et al*. 2010. Moisture variability in the southwestern United States linked to abrupt glacial climate change. *Nature Geoscience* **3**: 110-113.

Ward DW, Anderson RS, Briner JP *et al*. 2009. Numerical modeling of cosmogenic deglaciation records, Front Range and San Juan mountains, Colorado. *Journal of Geophysical Research–Earth Surface* 114: F01026.

Widmann BL, Kirkham RM, Houck KG *et al*. 2007. Geologic map of the Fairplay West Quadrangle, Park County, Colorado. Colorado Geological Survey Open File Report 06-7.

Young NE, Briner JP, Leonard EM *et al*. 2011. Assessing climatic and non-climatic forcing of Pinedale glaciation and deglaciation in the western U.S. Geology **39:** 171-17

FIGURES

Figure 1. (a) Location of the study area and surrounding mountain ranges. Area outlined in white is that shown in (b). (b) Stations used for modern climate data. Abbreviations: AV Arkansas Valley, BJ Buckskin Joe, BV Buena Vista, C Climax, F Fairplay, EM Elks Mountains, FP Fremont Pass, HP Hoosier Pass, JH Jones Hill, Leadville (2 stations), MC Michigan Creek, RD Red Deer, RT Rough and Tumble, S Salida, SL Sugarloaf Reservoir, SP South Park, SR Sawatch Range, and TL Twin Lakes Reservoir.

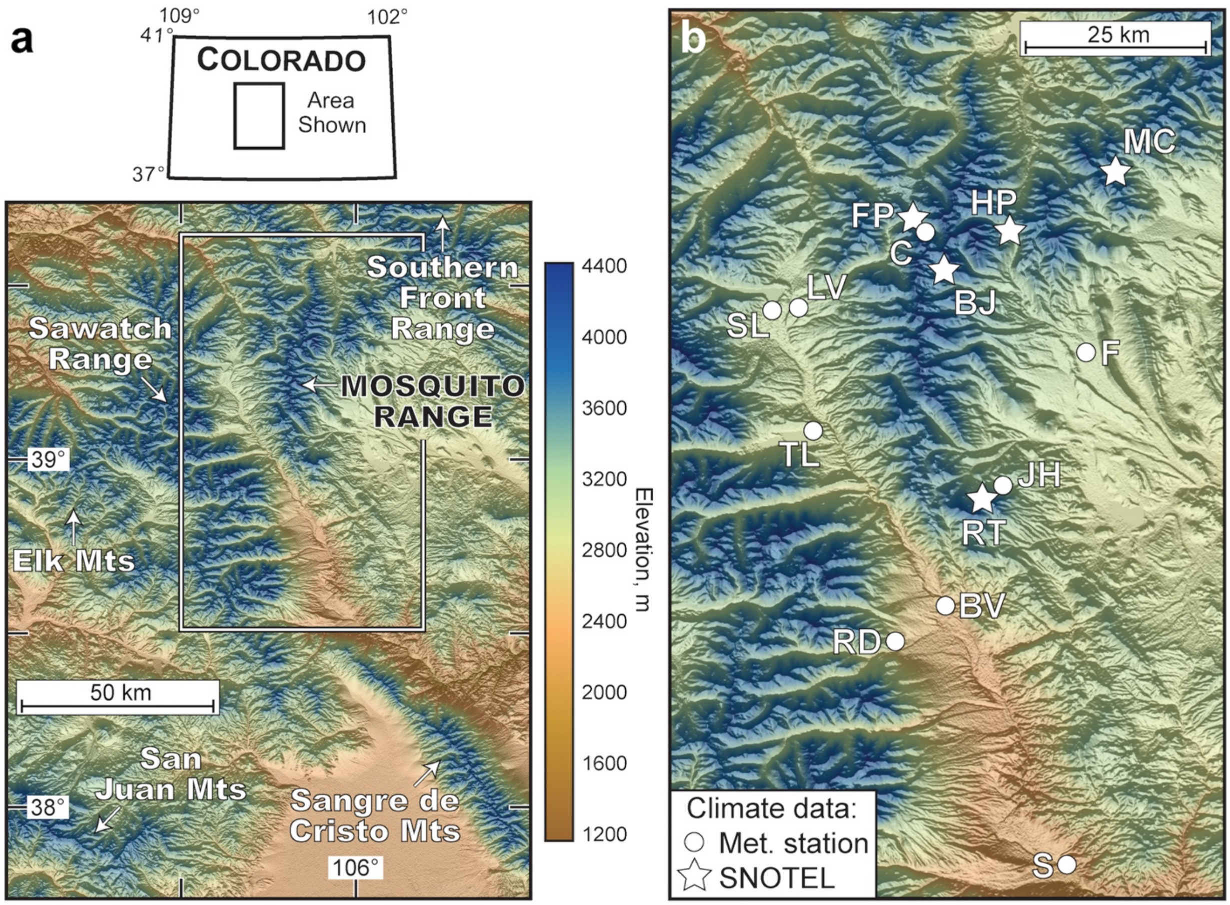

768 **Figure 2.** (a) Reconstructed glaciers of the Mosquito Range during their maximum Pinedale extent. A
769 more detailed example is shown in (b). Locations of moraine complexes sampled for surface exposure
770 dating are also shown in (a) and correspond to the areas shown in Figure 4.

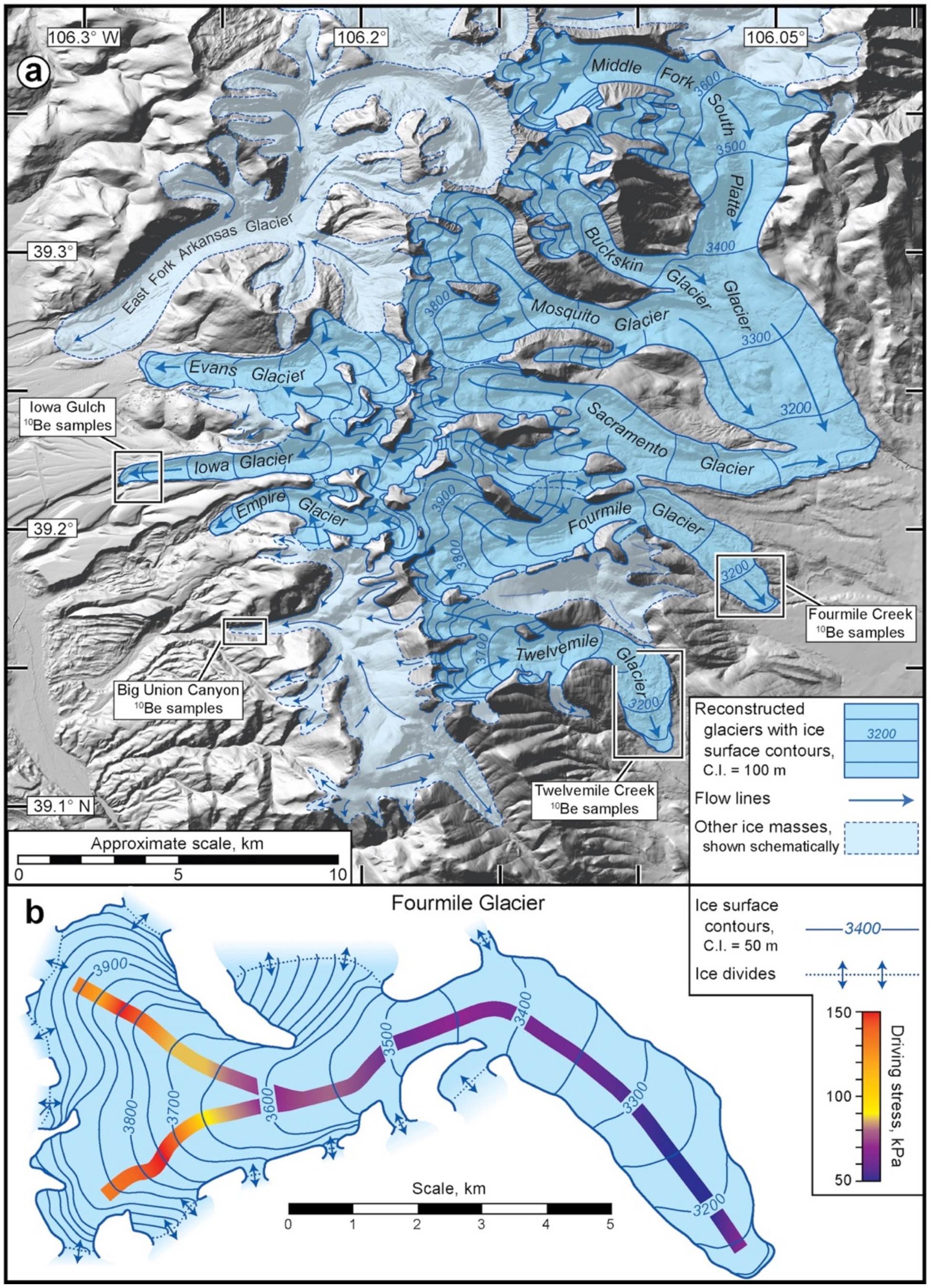

Figure 3. (a) Monthly distribution of precipitation at similar high and low elevations on the eastern and western slope of the Mosquito Range. Leadville data is a composite of two records. (b) Variation of winter precipitation with elevation on the eastern and western slopes of the Mosquito range. Two regressions are shown for the western side, one with and one without the Fremont Pass SNOTEL (FP) data. See text for discussion.

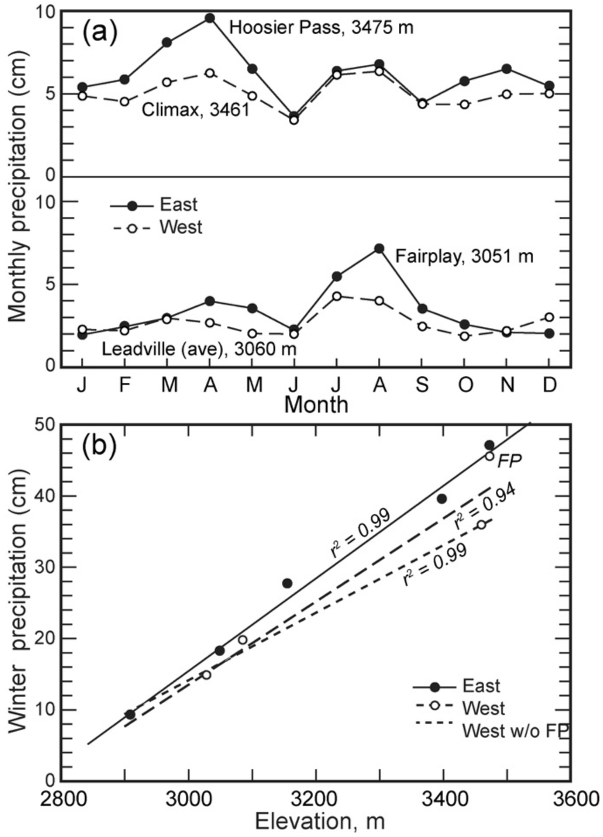

Figure 4. Locations of moraine boulders sampled for cosmogenic exposure dating and ^{10}Be ages (ka) in (a) Iowa Gulch, (b) Union Canyon, (c) Twelvemile Creek, and (d) Sacramento Creek and (e) Fourmile Creek. Moraine extents and ice margins are simplified and approximate. As noted in the text, boulders appropriate for sampling on several of the moraines were very scarce.

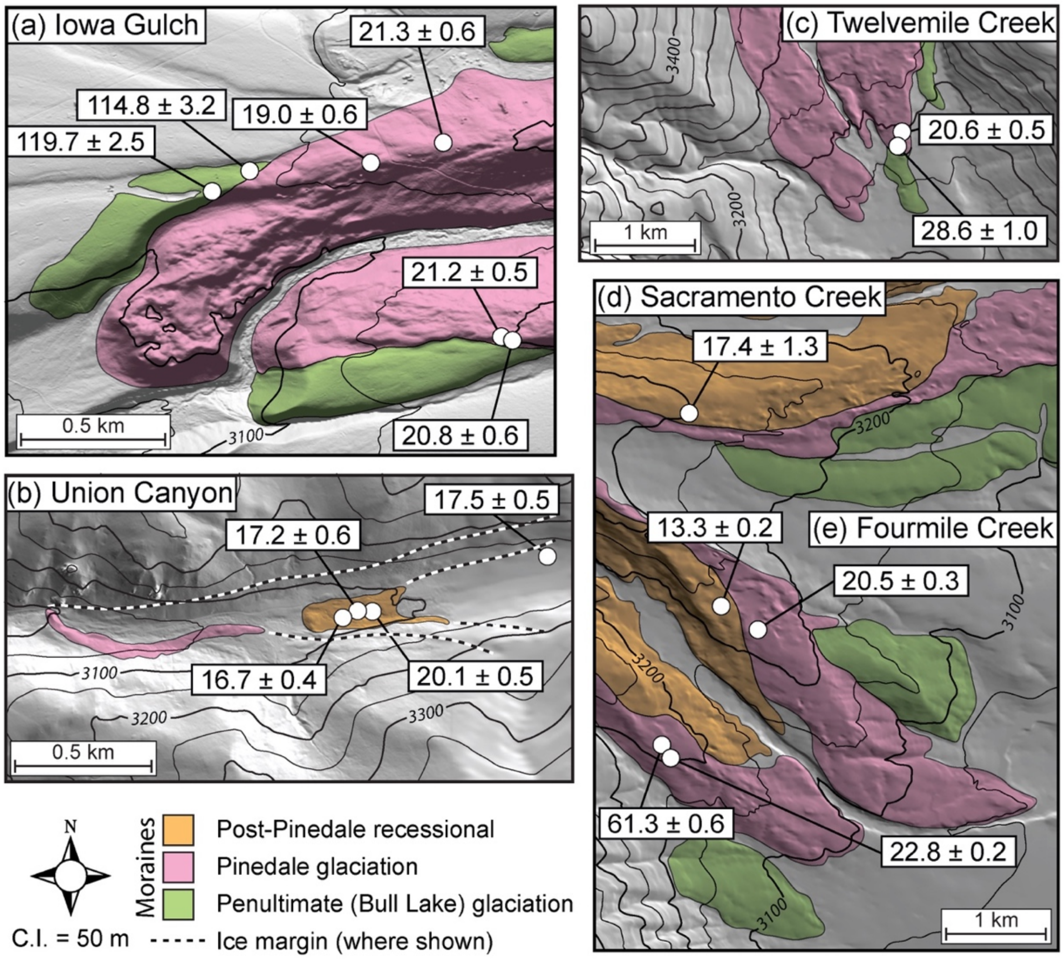

Figure 5. Comparison of modeled (a and b) monthly temperature, (c and d) monthly precipitation, and (e and f) snowpack evolution with observed records at various location in or near the study area. Shaded areas in (a-d) highlight the ablation and accumulation seasons respectively. In (e) the shaded area in the synthetic record for snowpack evolution at the Climax site shows possible range based on assumed snow density. In (f) the uncertainly associated with m_f values (dashed lines) is only shown for the Hoosier Pass site. See text for discussion.

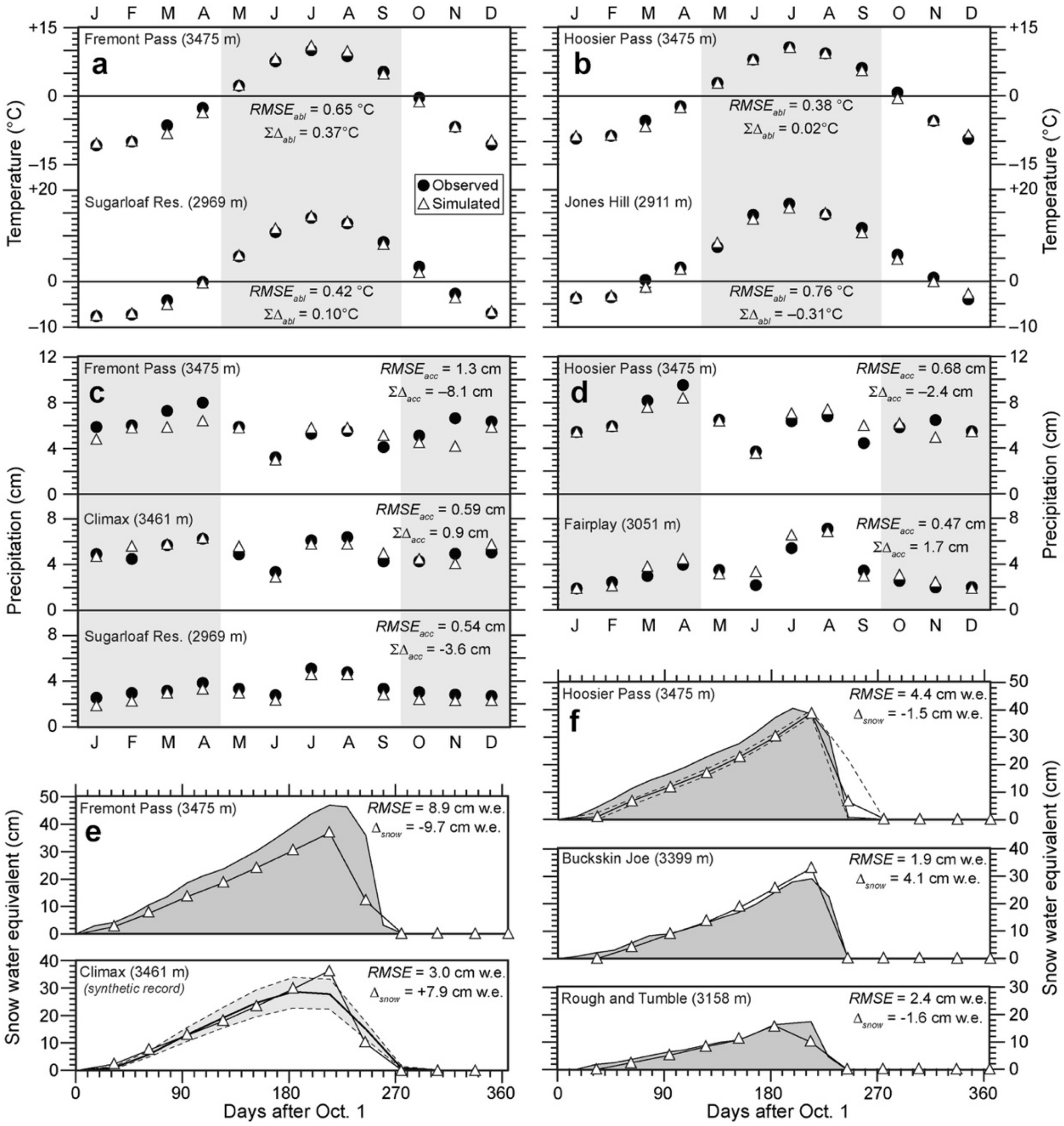

Figure 6. Combinations of temperature depression and changes in precipitation required to maintain steady-state mass balances of paleoglaciers at their maximum Pinedale extents. Mean values for glaciers on on eastern and western slopes are shown; standard deviation for each is ± 0.3 °C. The shaded area represents the more likely conditions in the region of the study area based on climate reconstructions. See text for discussion.

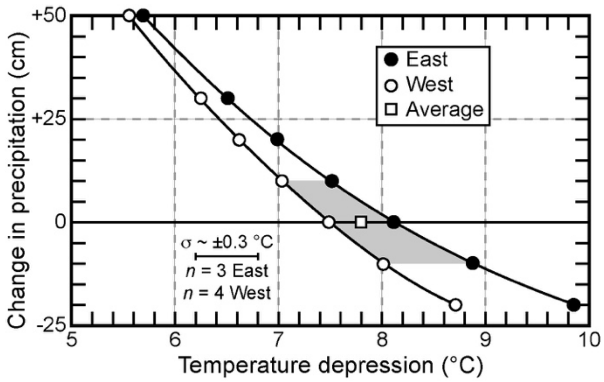

Figure 7. (a) Probability density plots of [10]Be ages for individual moraines and composite for all samples shown. Uncertainties shown reflect 1σ internal uncertainty. (b) North Greenland Ice Project ice core record of $\delta^{18}O$ variations with GICC05 chronology (LOESS smoothed; Rasmussen et. al, 2006). (c) Timing of the dominant highstand of pluvial lakes in the Great Basin (Munroe and Laabs, 2013). $\delta^{18}O$ variation from (d) Cave of the Bells, AZ (Wagner et al., 2010), (e) Fort Stanton Cave, NM (Asmerom et al., 2010), and (f) Devils Hole, NV (Moseley et al., 2016). (g) January and July insolation anomaly at 39° N (Berger, 1992). Vertical gray bars are the Heinrich Stadial (H1; taken here as ~18-15 ka) and the Younger Dryas (YD) event.

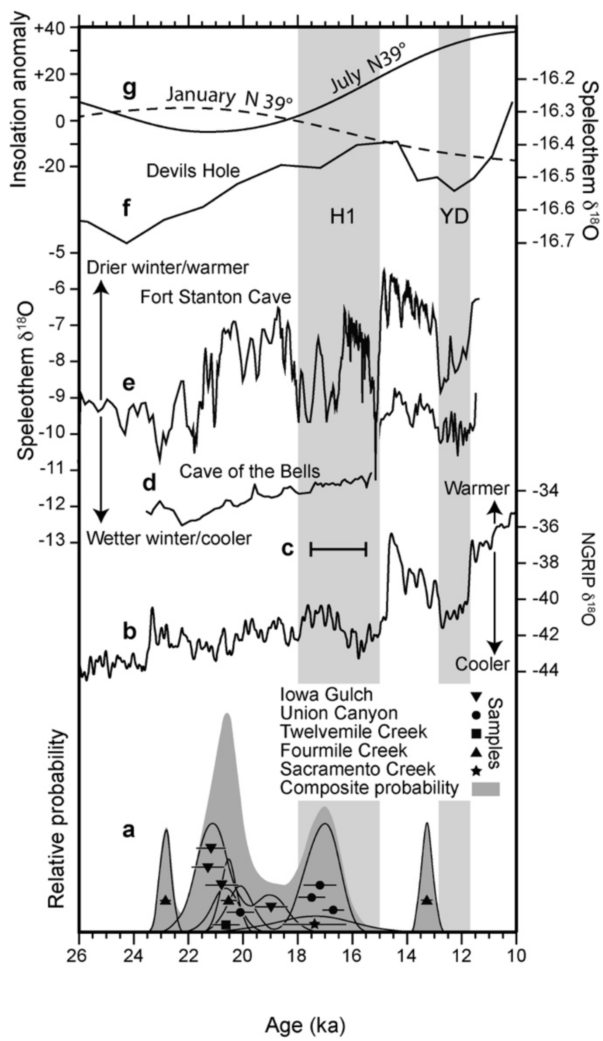

Table 1. Modern climate data* used in the model and derived values.

Station†	Elevation (m)	Mean Temperatures (°C)				Precipitation (cm)				
		Annual	T_{jul}	T_{jan}	H (T_{jul} - T_{jan})	Mean annual	Seasonal W	S	S	F
East slope										
Jones Hill	2911	5.3	16.8	–3.9	20.7	34.3	2.4	7.8	18.8	6.2
Fairplay	3051					39.8	6.4	10.4	14.8	8.1
Rough and Tumble‡	3158	2.9	12.9	–6.3	19.2	51.6	8.4	16.8	16.0	10.4
Michigan Creek	3230	1.9	12.1	–6.4	18.5					
Buckskin Joe‡	3399					70.4	15.2	18.9	20.1	16.2
Hoosier Pass‡	3475	0.3	10.3	–9.4	19.7	74.7	16.8	24.2	16.9	16.8
Mean value					*19.5*					
	dT_{jan}/dz (°C m^{-1}) =			*–0.0098*		*dP_{mod}/dz (cm m^{-1}) =*	*0.026*	*0.027*	*0.003*	*0.020*
		r^2 =		*0.95*			*0.99*	*0.93*	*0.13*	*0.99*
West slope										
Salida‡	2182	7.4	19.2	–3.1	22.3					
Buena Vista‡	2422	6.9	18.7	–3.4	22.1					
Red Deer	2682	5.7	16.8	–3.6	20.4	26.6	1.3	8.0	11.1	6.2
Twin Lakes‡	2804	3.1	14.7	–7.3	22.0	25.2	3.2	5.7	10.5	5.8
Sugarloaf Reservoir‡	2969	2.2	13.7	–7.6	21.3	41.7	8.4	10.5	13.5	9.4
Leadville 2SW	3031	1.6	12.7	–8.4	21.1	29.4	5.5	6.7	11.0	6.2
Leadville	3088	1.7	13.3	–8.3	21.6	33.7	9.3	8.3	9.4	6.6
Climax‡	3461	–0.8	11.1	–10.2	21.3	60.9	14.4	16.9	15.9	13.7
Fremont Pass‡	3475	–1.2	10.0	-11.0	21.0	69.3	18.3	21.2	14.0	15.8
Mean value					*21.5*					
	dT_{jan}/dz (°C m^{-1}) =			*–0.0065*		*dP_{mod}/dz (cm m^{-1}) =*	*0.019*	*0.017*	*0.005*	*0.012*
		r^2 =		*0.91*			*0.95*	*0.81*	*0.60*	*0.84*

* Different subsets of data were excluded from derivations of lapse rates dT_{jan}/dz and vertical precipitation gradients dP_{mod}/dz owing to (1) lack of data, (2) being extreme outliers and/or poor quality, or (3) inappropriate geographic location or elevation. Precipitation data is less inclusive under the assumption that precipitation is more variable over the region for than is temperature for given elevation.

†Location and station type shown in Fig. 1.

‡1981-2010 climate norm.

Table 2. Summary of geometric parameters associated with the reconstructed glaciers.

Glacier	Area (km^2)	Length* (km)	Average thickness† (m)	Maximum thickness† (m)
East slope				
Twelvemile	20.6	8.0	90	130
Fourmile	29.1	13.9	135	170
Sacramento	33.5	14.4	135	205
South Platte (glacier complex: Mosquito, Buckskin, and Middle Fork of the South Platte glaciers)	113.5	23.3	210	300
West slope				
Empire	9.2	7.8	100	140
Iowa	14.7	11.0	130	175
Evans	18.1	9.4	115	155

*Longest flowline
†Nearest 5 m

Table 3. Cosmogenic ^{10}Be exposure ages of moraines (see Supporting Information for details).

Valley/Sample ID	^{10}Be exposure age (ka)	Internal uncert. (ka)	External uncert. (ka)
Union Canyon			
UC-03-16	16.7	0.4	0.8
UC-04-16	17.2	0.6	0.9
UC-01-16	17.5	0.5	0.8
UC-02-16	20.1	0.5	0.9
Twelvemile Creek			
TMC-01-16	20.6	0.5	1.0
TMC-02-16	28.6	1.0	1.5
Iowa Gulch			
Pinedale terminal			
IG-04-16	19.0	0.6	1.0
IG-05-16	20.8	0.6	1.0
IG-06-16	21.2	0.5	0.9
IG-03-16	21.3	0.6	1.0
Bull Lake terminal[1]			
IG-02-16	133.2	3.2	6.6
IG-01-16	126.9	4.0	6.8
Fourmile Creek			
FMC-1-2015	13.3	0.2	0.5
FMC-2-2015	20.5	0.3	0.8
FMC-3-2015	*61.3*	*0.6*	*2.4*
FMC-4-2015	22.8	0.2	0.9
Sacramento Creek			
SC-1-16	17.4	1.3	1.4

[1]Assumed erosion rate of 1 mm/kyr.

Table 4. Inferred LGM temperature depression based on temperature-index simulations.

Paleoglacier	*ΔT* (°C)			ELA* (m)	
	F = –10 cm	*F* = 0 cm	*F* = +10 cm	Steady-state	AAR-derived
East slope					
Twelvemile	–9.3	–8.5	–7.9	3445	3420
Fourmile	–8.7	–7.9	–7.3	3505	3480
Sacramento	–8.6	–7.9	–7.3	3510	3500
South Platte	–8.9	–8.2	–7.6	3480	3435
Means ± standard deviation	–8.9 ± 0.3	–8.1 ± 0.3	–7.5 ± 0.3	3485 ± 25	3460 ± 40
West slope					
Empire	–7.9	–7.4	–6.9	3590	3555
Iowa	–7.9	–7.4	–6.9	3590	3560
Evans	–8.2	–7.7	–7.3	3545	3520
Means ± standard deviation	–8.0 ± 0.2	–7.5 ± 0.2	–7.0 ± 0.2	3575 ± 25	3545 ± 20

*For *F* = 1.0 only; nearest 5 m.

Table 5. Regional estimates of LGM temperature depression.

Location*	Temperature depression, °C**	Methodology†	Reference
Mosquito Range	7.5 - 8.2	TI	*This study*
Northern Sawatch Range	6.2 - 7.5	TI	Brugger *et al.*, 2017; in prep
Sawatch Range/Elk Mountains	6.9 ± 0.6	TI	Brugger, 2010
Sawatch Range/Elk Mountains	7.0 - 9.0	ELA	Brugger and Goldstein, 1999
Sangre de Cristo Mountains	5.0 +1.5/-1.0	EBFM	Leonard *et al.*, 2017a
Sangre de Cristo Mountains	6.0 - 7.5	ELA	Refsnider *et al.*, 2009
Sangre de Cristo Mountains	7.0 - 8.0	TI	Brugger *et al.*, 2009
Front Range	4.5 - 5.8	FM	Dühnforth and Anderson, 2011
Colorado Rocky Mountain region	7.6 ± 0.7	ELA	Leonard, 2007
Colorado Rocky Mountain region	8.5	ELA	Leonard, 1989

*Locations shown in Figure 1.
**Assuming no change in precipitation.
†TI = temperature-index model; ELA = climatic interpretation at glacier ELAs; EBFM = coupled energy-balance and glacier flow model; FM = flow model